Environmental Pollution 286 (2021) 117577

Contents lists available at ScienceDirect

Environmental Pollution

journal homepage: www.elsevier.com/locate/envpol

Source apportionment of $PM_{2.5}$ and sulfate formation during the COVID-19 lockdown in a coastal city of southeast China☆

Youwei Hong [a,b,c,d], Xinbei Xu [a,b,c,d], Dan Liao [e], Ronghua Zheng [a,b], Xiaoting Ji [a,b,c], Yanting Chen [a,b], Lingling Xu [a,b], Mengren Li [a,b], Hong Wang [g], Hang Xiao [a,b], Sung-Deuk Choi [f], Jinsheng Chen [a,b,*]

[a] Center for Excellence in Regional Atmospheric Environment, Institute of Urban Environment, Chinese Academy of Sciences, Xiamen, 361021, China
[b] Key Lab of Urban Environment and Health, Institute of Urban Environment, Chinese Academy of Sciences, Xiamen, 361021, China
[c] University of Chinese Academy of Sciences, Beijing, 100049, China
[d] College of Resources and Environment, Fujian Agriculture and Forest University, Fuzhou, 350002, China
[e] College of Environment and Public Health, Xiamen Huaxia University, Xiamen, 361024, China
[f] Department of Urban and Environmental Engineering, Ulsan National Institute of Science and Technology, Ulsan, 44919, South Korea
[g] Fujian Meteorological Science Institute, Fujian Key Laboratory of Severe Weather, Fuzhou, 350001, China

ARTICLE INFO

Keywords:
$PM_{2.5}$
Source apportionment
Transition-metal ion catalyzed oxidation
Sulfate
COVID-19

ABSTRACT

Revealing the changes in chemical compositions and sources of $PM_{2.5}$ is important for understanding aerosol chemistry and emission control strategies. High time-resolved characterization of water-soluble inorganic ions, elements, organic carbon (OC), and elemental carbon (EC) in $PM_{2.5}$ was conducted in a coastal city of southeast China during the COVID-19 pandemic. The results showed that the average concentration of $PM_{2.5}$ during the city lockdown (CLD) decreased from 46.2 μg m^{-3} to 24.4 μg m^{-3}, lower than the same period in 2019 ($PM_{2.5}$: 37.1 μg m^{-3}). Concentrations of other air pollutants, such as SO_2, NO_2, PM_{10}, OC, EC, and BC, were also decreased by 27.3%–67.8% during the CLD, whereas O_3 increased by 28.1%. Although SO_2 decreased from 4.94 μg $m^{-3}$to 1.59 μg m^{-3} during the CLD, the concentration of SO_4^{2-} (6.63 μg m^{-3}) was comparable to that (5.47 μg m^{-3}) during the non-lockdown period, which were attributed to the increase (16.0%) of sulfate oxidation rate (SOR). O_x (O_3+NO_2) was positively correlated with SO_4^{2-}, suggesting the impacts of photochemical oxidation. A good correlation ($R^2 = 0.557$) of SO_4^{2-} and Fe and Mn was found, indicating the transition-metal ion catalyzed oxidation. Based on positive matrix factorization (PMF) analysis, the contribution of secondary formation to $PM_{2.5}$ increased during the epidemic period, consisting with the increase of secondary organic carbon (SOC), while other primary sources including traffic, dust, and industry significantly decreased by 9%, 8.5%, and 8%, respectively. This study highlighted the comprehensive and nonlinear response of chemical compositions and formation mechanisms of $PM_{2.5}$ to anthropogenic emissions control under relatively clean conditions.

1. Introduction

The multi-phase chemistry of fine particulate matter ($PM_{2.5}$) has attracted atmospheric scientists because it affects human health and climate change by triggering urban haze pollution and radiative forcing (Su et al., 2020; Zheng et al., 2020a). Due to association with aerosol precursor emissions, atmospheric chemistry, and meteorology, the formation mechanism of $PM_{2.5}$ is still complex (Ding et al., 2019; Huang et al., 2020b; Liu et al., 2019a; Wang et al., 2014; Zhang et al., 2019). Some studies have reported that the formation of secondary sulfate include the gas-phase oxidation by OH radical and the aqueous oxidation by H_2O_2, O_3, organic peroxides, and transition metal ions (TMIs) catalyzed O_2 (Harris et al., 2013; Wang et al., 2016; Li et al., 2020; Wang et al., 2020a; Wang et al., 2021). However, the formation and contribution of secondary sulfate to haze episodes in urban areas is not fully understood.

An outbreak of a novel coronavirus disease (COVID-19) in December 2019, China firstly implemented a national emergency response,

☆ This paper has been recommended for acceptance by Da Chen.

* Corresponding author. Institute of Urban Environment, Chinese Academy of Sciences, 1799 Jimei Road, Xiamen, 361021, China.
E-mail address: jschen@iue.ac.cn (J. Chen).

https://doi.org/10.1016/j.envpol.2021.117577
Received 19 January 2021; Received in revised form 7 June 2021; Accepted 9 June 2021
Available online 11 June 2021

including suspending public transport and banning public gatherings, and then other countries further tighten social distancing measures (Kraemer et al., 2020; Saraswat and Saraswat, 2020; Tian et al., 2020). This provides a good opportunity to evaluate the responses of $PM_{2.5}$ formation to a dramatic emission reduction of its precursors (Chen et al., 2020; Liu et al., 2020a; Pei et al., 2020; Stratoulias and Nuthammachot, 2020). Until now, many studies have reported that air quality has been improved significantly during the city lockdown (CLD) period (Collivignarelli et al., 2020; He et al., 2020; Miyazaki et al., 2020; Rodriguez-Urrego and Rodriguez-Urrego, 2020; Sharma et al., 2020; Zangari et al., 2020). In contrast, haze pollution driven by the increase of atmospheric oxidizing ability still occurs, due to unfavorable meteorological conditions (Chang et al., 2020; Le et al., 2020). Therefore, there is a need to deeply understand the formation mechanism of $PM_{2.5}$ and its response to the reduction of precursors during the CLD period (Sun et al., 2020; Zheng et al., 2020b).

Affected by seasonal monsoon and aerosol precursor emissions from intense human activities, coastal cities in the southeast of China have experienced occasional air pollution in recent years (Liu et al., 2020b; Wu et al., 2020). Our previous studies mainly focused on the pollution characteristics and sources of $PM_{2.5}$ in this region (Liu et al., 2020b; Wu et al., 2019; Xu et al., 2018). The COVID-19 outbreak led to anthropogenic emission reductions including traffic, industry and resident life around the country (Jia et al., 2020; Singh et al., 2020; Zhao et al., 2020). Hence, it offered a unique opportunity to study the interactions among aerosol precursor reduction, heterogeneous chemistry, and meteorology. The objective of this study is to better understand the sources and formation mechanisms of $PM_{2.5}$ during the COVID-19 lockdown in coastal areas. Therefore, we set out to (1) characterize the variations of criteria air pollutants concentrations before, during, and after the CLD period; (2) qualify different source contributions to $PM_{2.5}$ using the positive matrix factorization (PMF) analysis; (3) explore the formation mechanism of SO_4^{2-} for emissions control in coastal city.

2. Methods and materials

2.1. Study area

The monitoring site (Institute of Urban Environment, Chinese Academy of Sciences in Xiamen, a coastal city of southeast China, 118.06° E, 24.61° N) is located on the interface between land and the sea. The air-monitoring supersite is setup on the rooftop of one building, which is surrounded by residential buildings, educational institutions, commercial zone, and freeways. There is no industrial source nearby, and the site is representative of an urban environment. Downtown in Xiamen with densely populated and traffic jams was located in the south of IUE. Criteria air pollutants, chemical compositions in $PM_{2.5}$, and meteorological parameters were continuously measured online before (from Jan 6 to Jan 23), during (from Jan 24 to Feb 10), and after (from Feb 11 to Feb 26) the city lockdown (CLD) in 2020.

2.2. Observation

Hourly mass concentrations of $PM_{2.5}$ and PM_{10} were measured by using a tapered element oscillating microbalance (TEOM1405, Thermo Scientific Corp., MA, USA). NO_2, SO_2, and O_3 were monitored using continuous gas analyzers (TEI 42i, 43i, and 49i, Thermo Scientific Corp., MA, USA). Ambient meteorological parameters including relative humidity (RH), temperature (T), wind speed (WS), and wind direction (WD) were obtained by an ultrasonic atmospherium (150WX, Airmar, the USA). Water-soluble inorganic ions (WSII) in $PM_{2.5}$ (Cl^-, SO_4^{2-}, NO_3^-, Na^+, K^+, NH_4^+, Mg^{2+}, and Ca^{2+}) were hourly measured using a Monitoring device for AeRosols and Gases in ambient Air (MARGA 2080; Metrohm Applikon B.V.; Delft, Netherlands). Simultaneously, organic carbon (OC) and elemental carbon (EC) in $PM_{2.5}$ were measured using a OC/EC analyzer (model RT-4; Sunset Laboratory Inc.; Tigard, USA) (Chang et al., 2020). BC was monitored using an Aethalometer (AE31, Magee Scientific, USA) with a $PM_{2.5}$ cut-off inlet. Besides, concentrations of 22 elements (Al, Si, S, Fe, K, Mn, Pb, Ca, Zn, Ba, V, Cu, Ni, As, Cr, Ag, Se, Br, Hg, Sn, Ti, and Sb) were measured by a multi-metal monitor (Xact™ 625; Cooper Environmental Services, LLT; Portland, USA). The method detection limits (MDLs) for these elements are shown in Table S2. To investigate atmospheric new particle growth in the coastal city, a scanning mobility particle sizer (SMPS, model 3938, TSI, Inc., USA) was operated to measure number size distributions of 3–736 nm particles at a time resolution of 5 min. The maintenance/accuracy of all online instruments was validated according to our previous studies (Hu et al., 2020; Wu et al., 2019).

2.3. Positive matrix factorization (PMF) analysis

The PMF 5.0 model was applied to quantify high-time-resolution sources of $PM_{2.5}$ during the pandemic periods. The details of the model analysis were described in our previous studies (Liu et al., 2020b). Briefly, Eq. (1) demonstrates j compound species in the ith sample as the concentration from p independent sources.

$$x_{ij} = \sum_{k=1}^{p} g_{ik} f_{ki} + e_{ij} \quad (1)$$

Where e_{ij} is the residual for each species, f_{kj} is the jth species fraction from the kth source, g_{ik} is the species contribution of the kth source to the ith sample, x_{ij} is the jth species concentration measured in the ith sample, and p is the total number of independent sources. Data below the detection limit were held with the associated uncertainty adjusted. The Q (Eq. (2)) based on the uncertainties (μ) was used to evaluate the steadiness of the solution.

$$Q = \sum_{i=1}^{n} \sum_{j=1}^{m} \left[\frac{x_{ij} - \sum_{k=1}^{p} g_{ik} f_{kj}}{\mu_{ij}} \right]^2 \quad (2)$$

2.4. Backward trajectory analysis

Hybrid Single-Particle Lagrangian Integrated Trajectory (HYSPLIT) was applied to analyze the air masses before, during and after the CLD. The 72-h backward trajectories at a height of 100 m were run every hour. Cluster analysis was performed and four clusters were determined according to the total spatial variance (TSV). A detailed method of the HYSPLIT analysis can be referred to our previous studies (Liu et al., 2020b; Zhang et al., 2017b).

2.5. Potential source contribution function (PSCF)

The PSCF values were calculated to identify potential source areas contributing to the concentrations of $PM_{2.5}$ and SO_4^{2-} before, during and after the CLD. PSCF values were defined as the conditional probability which was related to the passage of air parcels through the grid cell to the receptor site (Hopke et al., 1995). The zone of concern is divided into i × j grid cells. The PSCF value is normalized as follows:

$$PSCF_{ij} = m_{ij} / n_{ij} \quad (3)$$

where m_{ij} is the number of endpoints higher than a given threshold for ij-th cell and n_{ij} is the total number of endpoints in the ij-th cell. In this study, annual average concentrations of $PM_{2.5}$ and SO_4^{2-} were treated as the threshold criteria, and the average number of endpoints per cell n_{ave} was 3 (Zhang et al., 2017b). A weighting function wij was multiplied with the PSCF values to minimize the uncertainty (Polissar et al., 1999), as follow:

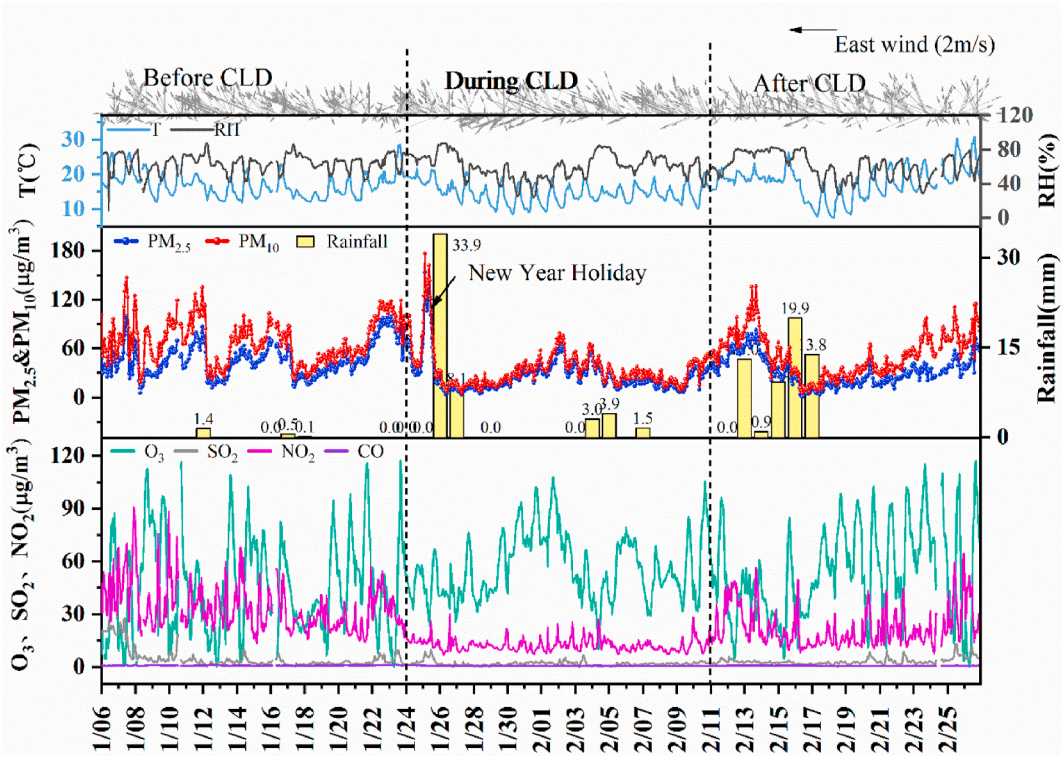

Fig. 1. Time series of criteria air pollutants and meteorological parameters before, during, and after the city lockdown (CLD).

Table 1
Concentration of $PM_{2.5}$ and its components (μg m^{-3}), criteria air pollutants and meteorological parameters before, during and after the city lockdown (CLD).

	Before CLD	During CLD	After CLD	Fireworks
$PM_{2.5}$	46.2 ± 20.9	24.4 ± 13.7	32.4 ± 17.9	77.4 ± 40.4
PM_{10}	68.9 ± 27.1	31.6 ± 16.7	52.0 ± 26.2	92.0 ± 44.5
O_3	44.4 ± 28.3	56.8 ± 18.7	53.7 ± 26.5	48.0 ± 12.2
CO	0.77 ± 0.15	0.56 ± 0.11	0.59 ± 0.14	0.67 ± 0.10
SO_2	4.94 ± 5.71	1.59 ± 0.97	3.13 ± 1.95	5.06 ± 2.21
NO_2	34.2 ± 13.5	12.2 ± 3.55	22.3 ± 11.1	14.6 ± 3.10
BC	1.74 ± 0.86	0.80 ± 0.44	1.15 ± 0.60	1.01 ± 0.23
OC	11.34 ± 3.84	6.10 ± 3.21	6.54 ± 2.17	9.66 ± 4.24
EC	1.80 ± 0.91	0.90 ± 0.70	1.20 ± 0.50	0.97 ± 0.33
SO_4^{2-}	6.63 ± 2.94	5.47 ± 2.94	4.79 ± 2.74	15.35 ± 9.33
NO_3^-	11.93 ± 6.78	4.17 ± 3.44	6.97 ± 5.29	6.88 ± 1.88
NH_4^+	5.58 ± 3.03	2.58 ± 1.87	3.57 ± 2.64	2.34 ± 0.50
Na^+	0.10 ± 0.09	0.04 ± 0.06	0.11 ± 0.15	0.17 ± 0.06
K^+	0.20 ± 0.85	0.23 ± 0.39	0.10 ± 0.11	11.21 ± 8.55
Mg^{2+}	0.01 ± 0.02	0.04 ± 0.07	0.01 ± 0.01	1.79 ± 1.32
Ca^{2+}	0.07 ± 0.08	0.02 ± 0.04	0.03 ± 0.06	0.02 ± 0.03
SIA	23.0 ± 14.4	12.70 ± 8.58	15.1 ± 11.4	44.9 ± 25.9
NO_3^-/SO_4^{2-}	1.80 ± 0.64	0.79 ± 0.39	1.43 ± 0.77	0.62 ± 0.32
NOR	0.21 ± 0.09	0.19 ± 0.10	0.18 ± 0.11	0.26 ± 0.05
SOR	0.69 ± 0.19	0.80 ± 0.10	0.65 ± 0.13	0.77 ± 0.07
$PM_{2.5}/PM_{10}$	0.66 ± 0.09	0.77 ± 0.11	0.62 ± 0.12	0.82 ± 0.06
T(°C)	16.88 ± 3.40	14.67 ± 2.87	17.71 ± 4.56	18.70 ± 1.50
RH(%)	63.8 ± 10.6	60.3 ± 13.9	61.2 ± 14.6	68.3 ± 4.32
P(kPa)	100.9 ± 0.24	101.1 ± 0.33	101.1 ± 0.48	100.9 ± 0.17
WS(m/s)	1.42 ± 0.68	1.62 ± 0.79	1.30 ± 0.74	1.09 ± 0.29

$$w_{ij} = \begin{cases} 1.00 & n_{ij} > 3n_{ave} \\ 0.70 & 1.5n_{ave} < n_{ij} \le 3n_{ave} \\ 0.42 & n_{ave} \le n_{ij} \le 1.5n_{ave} \\ 0.17 & n_{ij} \le n_{ave} \end{cases} \quad (4)$$

3. Results and discussions

3.1. Overview of criteria air pollutants

Time series of criteria air pollutants and meteorological factors before, during, and after the city lockdown (CLD) are shown in Fig. 1. The mean concentrations of $PM_{2.5}$ during the CLD decreased from 46.2 μg m^{-3} to 24.4 μg m^{-3} and then back to 32.4 μg m^{-3} after the CLD (Table 1). The concentrations of other air pollutants, such as SO_2, NO_2, PM_{10}, OC, EC, and BC, also showed a decreasing trend (by 27.3%–67.8%) during the CLD, whereas only O_3 increased (by 28.1%). In contrast, the concentrations of SO_2, PM_1, $PM_{2.5}$, PM_{10}, and CO during the same periods in 2018 and 2019 were not significantly changed (Table S2). The little peak of NO_2 concentrations during the CLD was attributed to the impact of stationary combustion sources such as the coal-fired power plant, and the concentration of secondary components (SO_4^{2-}, NO_3^-, and NH_4^+) in $PM_{2.5}$ occasionally increased, especially in a relatively stable atmospheric condition. For the CLD, the temporal pattern of air pollutants was consistent with the fact that the emissions from anthropogenic activities were reduced. Similar results have been reported in other cities such as Beijing, Shanghai, and Wuhan (He et al., 2020; Wang et al., 2020b). After the outbreak of COVID-19, the local government has taken unprecedented control measures, including restricting transportation and public gathering (Kraemer et al., 2020; Tian et al., 2020). Satellite observations also showed reduced NO_2 emissions over Chinese cities, ranging from 11% to 69% (Bauwens et al., 2020; Liu et al., 2020a). Wuhan was the first city in China to adopt the lockdown measures, which improved the air quality accordingly (Zheng et al., 2020b). Meanwhile, the increased contribution of combustion and secondary organic aerosol to $PM_{2.5}$ was reported (Zheng et al., 2020b; Huang et al., 2020a). Therefore, the response of the sources and

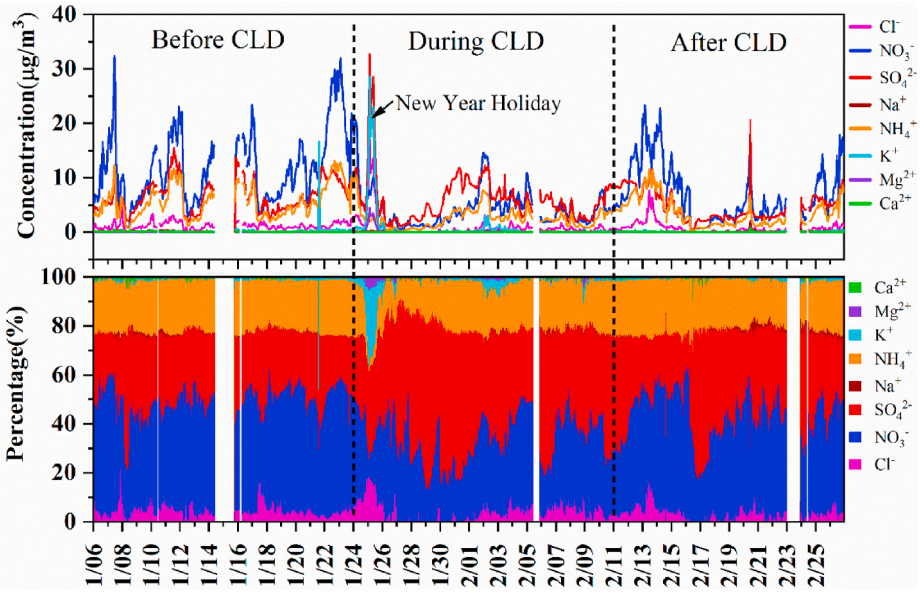

Fig. 2. Concentrations and percentages of water-soluble inorganic ions in $PM_{2.5}$ before, during, and after the city lockdown (CLD).

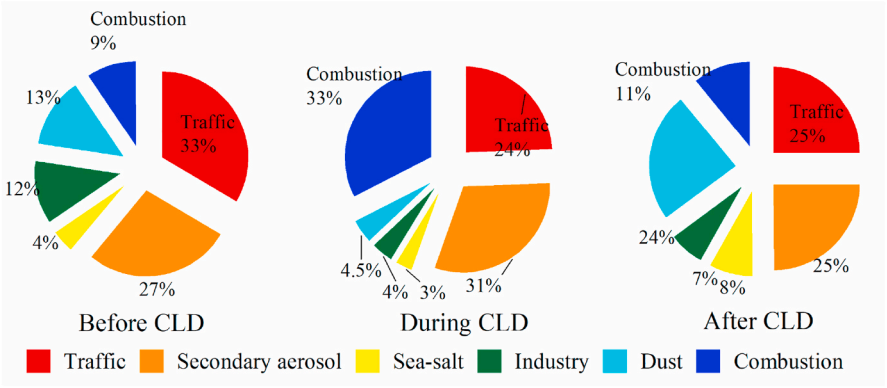

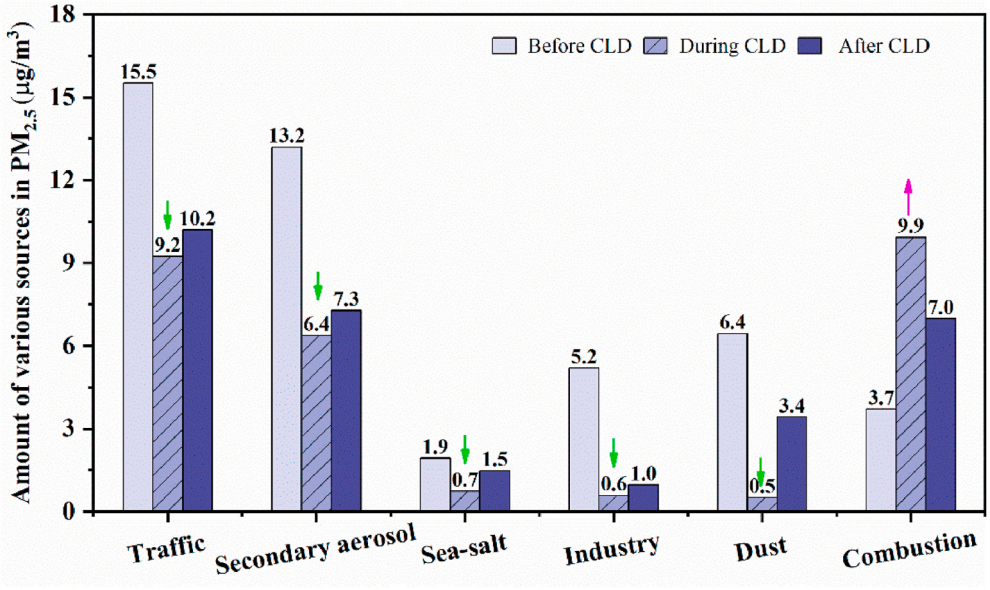

Fig. 3. Source contributions to $PM_{2.5}$ based on the PMF model analysis before, during, and after the city lockdown (CLD).

formation of $PM_{2.5}$ to aerosol precursor emissions control would be complex and nonlinear.

3.2. Chemical compositions of $PM_{2.5}$

The concentrations of SO_4^{2-}, NO_3^-, and NH_4^+ before the CLD were 6.63 ± 2.94 μg/m^3, 11.93 ± 6.78 μg/m^3, and 5.58 ± 3.03 μg/m^3, respectively (Table 1). During the CLD, the concentrations of NO_3^- and NH_4^+ sharply decreased, with an average concentration of 4.17 μg/m^3 and 2.58 μg/m^3, and increased to 6.97 μg/m^3 and 3.57 μg/m^3 after the CLD. Time series of water-soluble inorganic ions (WSII) in $PM_{2.5}$ are shown in Fig. 2. The mean concentrations of the total WSII before, during, and after the CLD was 23.1 μg/m^3, 12.7 μg/m^3, and 15.1 μg/m^3, respectively. During the CLD, sulfate was the most abundant species with a proportion of 43.1% of total WSII, followed by ammonium (26.6%) and nitrate (9.7%). However, the percentage of nitrate (41.5%) before the CLD was the biggest, followed by sulfate (28.8%) and ammonium (13.5%).

Organic carbon (OC) and elemental carbon (EC) levels during different periods were demonstrated in Table 1 and Fig. S1. Average OC and EC concentrations were 6.10 ± 3.21 and 0.90 ± 0.70 μg/m^3 during the CLD, ~50% lower than those (11.34 ± 3.84 and 1.80 ± 0.91 μg/m^3) before the CLD. As shown in Fig. S1, the proportion of SOC was relatively higher than those before and after the CLD, suggesting the influence of secondary formation. In addition, the average OC/EC (7.69 ± 3.16) during the CLD was slightly higher than those before and after the CLD (6.87 ± 1.85 and 6.06 ± 2.75, respectively).

Fig. S2 shows the variations of metal elements in $PM_{2.5}$ under different periods, based on hourly measurement concentrations. Most of them (including Fe, Ca, Si, Cr, Mn, Zn, Ni, and V) decrease during the CLD. An important explanation is that anthropogenic activities including traffic, industry, and port have little emissions, which was consistent with the reduction of SO_2, NO_2, and CO (Table 1). Previous studies have reported that traffic activities could enhance the concentrations of crustal elements (e.g., Fe, Ca, and Si) in $PM_{2.5}$ (Yu et al., 2019). However, Al did not significantly decrease during the CLD, which was related to contribution combustion sources such as fireworks displays. In addition, the concentrations of V and Ni during the CLD decrease from 0.7 ng/m^3 to 0.1 ng/m^3 and 3.1 ng/m^3 to 0.8 ng/m^3, respectively (Fig. S2). V and Ni are dominant elements in crude oil and are considered the tracers of ship emissions (Agrawal et al., 2008; Tao et al., 2017). The monitoring site is 10 km north of the Xiamen port, which is one of the top 10 ports in China. The shutdown of port activities during the CLD resulted in the reduction of V and Ni concentration at the monitoring site.

3.3. Sources apportionment of $PM_{2.5}$

The PMF model was applied to conduct high-time-resolution source apportionment of $PM_{2.5}$, based on online hourly measurement data. The factor profiles and the contribution of various sources to $PM_{2.5}$ are shown in Fig. 3, Fig.S4, and S5. The contributions of emission sources to $PM_{2.5}$ (except for combustion) significantly decreased during the epidemic period. In factor 1, K^+, Cl^-, S, and Ba are dominant and it is identified as combustion sources (Watson et al., 2001). During the CLD, the influence of combustion sources (e.g., biomass burning and coal combustion) significantly increased to 33%, contributing to $PM_{2.5}$ concentrations from 3.7 μg/m^3 to 9.9 μg/m^3. Firstly, during the cold season, residential daily stir-frying activities for cooking and solid fuel (e.g., crop residues, wood, and coal) burning for heating were dominant in the north of China (Kong et al., 2015; Zheng et al., 2020c). Secondly, the distribution of fire spots during the CLD was more active than those before the CLD (Fig. S6). Biomass burning could enhance the contribution of combustion to $PM_{2.5}$ at the monitoring site through long-range transport. Thirdly, the contribution of combustion source to $PM_{2.5}$ sharply increased from Jan 25, i.e., the Spring Festival in China, as

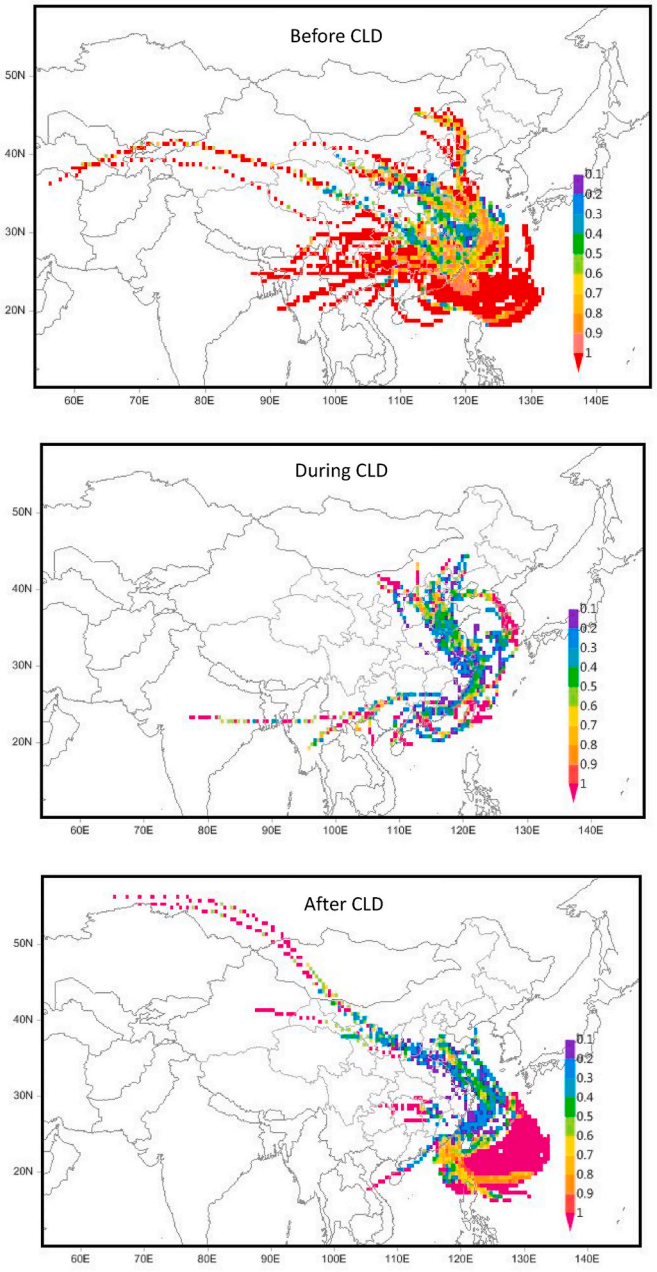

Fig. 4. Spatial distributions of PSCF for $PM_{2.5}$ before, during, and after the city lockdown (CLD).

shown in Fig. S5. The celebration activity, including scattered firework displays, was lasted for one week. The effects of firework displays during the New Year Holidays on $PM_{2.5}$ and its components and other air pollutants are shown in Table 1 and Fig. S3.

Previous studies had found that construction and road dust was characterized by a high loading of Al, Si, Ca^{2+}, Na^+, Mg^{2+}, and Zn (Han et al., 2007; Xu et al., 2018). In this study, the factor of dust (F2) was identified by high contributions of Si, Na^+, and Zn (Fig.S4). The PMF analysis showed that the contribution of dust to $PM_{2.5}$ sharply decreased from 13% to 4.5% during the CLD (Fig. 3). Factor 3, contributing to the high loading of metal elements (Mn, Zn, Ni, Pb, and As), was characterized by industrial emissions (Belis et al., 2019). The decreased contributions from 12% to 4% during the CLD were mainly attributed to the shutdown of industrial activities. The contributions of industry and dust to $PM_{2.5}$ before the CLD was 5.2 μg/m^3 and 6.4 μg/m^3, respectively. The shutdown of factories, and the reduction of road and construction dusts

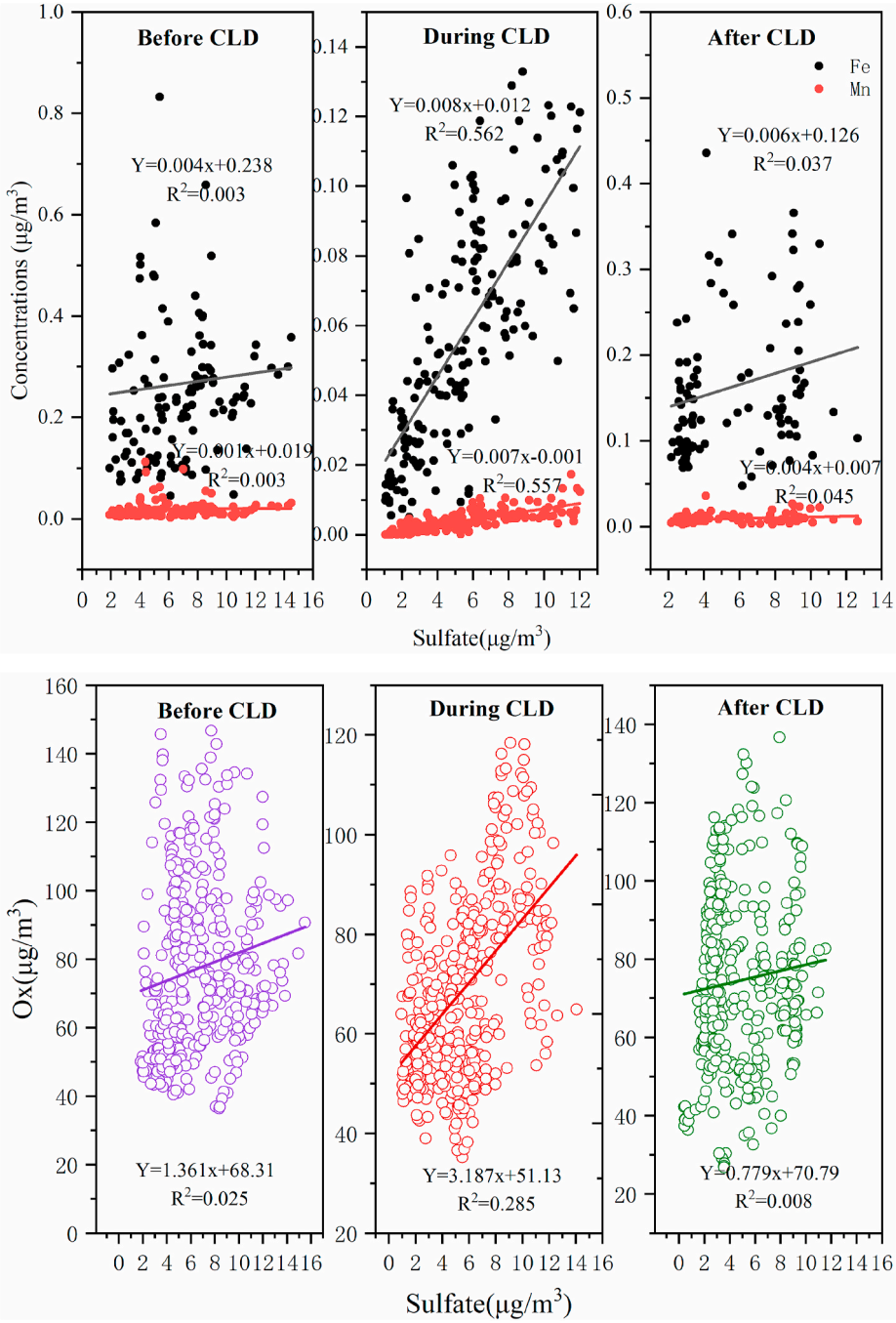

Fig. 5. Linear regression between SO_4^{2-} and Fe, Mn, Ox (O_3+NO_2) under different periods.

have sharply decreased the contribution of these sources. Factor 4, with the highest proportion of Na^+ loading, was related to the influence of sea-salt aerosol (Polissar et al., 1998). The percentages of sea-salt (3–8%) under different periods were relatively constant. Factor 5 was associated with secondary aerosol, with high loads of SO_4^{2-}, NO_3^-, and NH_4^+. The nitrate oxidation rate (NOR) and its precursor (NO_2) showed a descending trend (Table 1, Fig.S9), implying low fractions of nitrate due to secondary formation. Meanwhile, ammonium concentrations also have a similar pattern decreased from 5.58 μg/m^3 to 2.58 μg/m^3. However, the sulfate oxidation rate (SOR) showed enhancements during the CLD, and the fractions of sulfate from secondary formation were constant. The percentage of secondary aerosol increased during the CLD, according to the PMF analysis. Le et al. (2020) found that reduced nitrogen oxides caused O_3 enhancement, furthering facilitating secondary aerosol formation, and resulted in haze episodes in winter under high humidity and stagnant airflow conditions. Factor 6 shows high contributions of EC, OM, and Pb, which are generally indicators of vehicle exhaust (Xu et al., 2018). During the CLD, the restricted vehicle travel resulted in the reduced contribution of traffic to $PM_{2.5}$ from 15.5 μg/m^3 to 9.2 μg/m^3, although the percentages of traffic slightly decreased.

Spatial distributions of potential sources of $PM_{2.5}$ at the monitoring site are presented in Fig. 4. Before the CLD, significant potential source regions with high PSCF values mainly include the North China Plain, the YRD region, the south and southwest of China, and the southeast China sea. The results indicated the influence of emissions was from urban and industrial areas through long-range transport. Moderate and weak PSCF values were mainly distributed in East and Central China. During the CLD, potential source regions of $PM_{2.5}$ with high PSCF values were

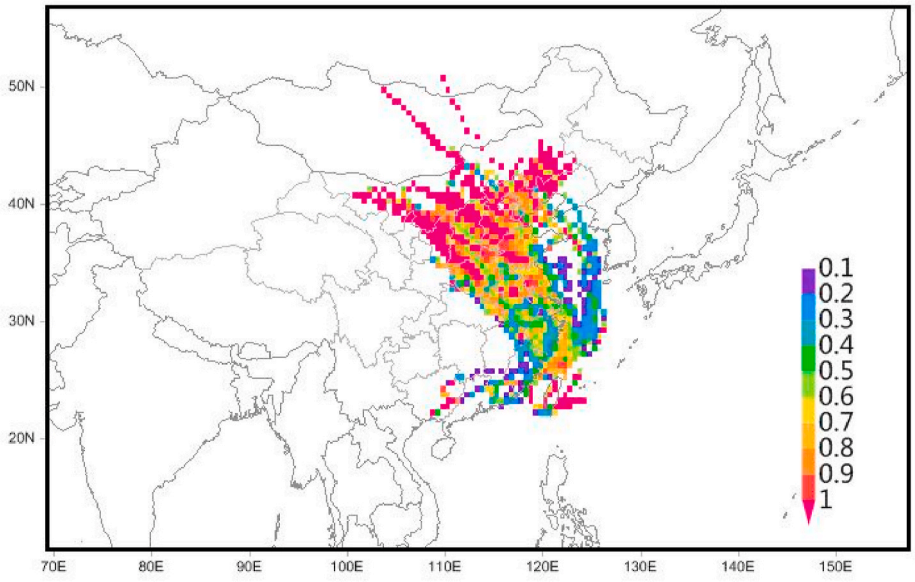

Fig. 6. Spatial distributions of PSCF for SO_4^{2-} during the city lockdown (CLD).

seldom observed. Moreover, the PSCF values from urban and industrial areas decreased. After the CLD, potential source regions of $PM_{2.5}$ with moderate and weak PSCF values are primarily affected by Northwest China and the Southeast China Sea. In this stage, factories and public transportation in Fujian province started to reopen, but some regions still have strict epidemic prevention and control.

During the CLD, the 72 h backward trajectory clusters for air mass and the corresponding concentrations of $PM_{2.5}$ and its components are shown in Fig.S7b. The northerly cluster (Cluster 4) was the most frequent, accounting for 38.5% of total air masses, followed by Cluster 2 (31.1%), Cluster 1 (27.2%), and Cluster 3 (3.2%). Cluster 1 and Cluster 3 represent the surrounding regions and long-range transport originating from western and southwestern of China, respectively. Cluster 2 came from the East China Sea and passed through the densely populated YRD region. The long-range northerly continental cluster (Cluster 4) passed over heavily polluted areas of North and Central China such as Hebei, Shandong, and Anhui provinces. Anthropogenic emissions strongly influenced Cluster 2 and 4, and Cluster 4 had the highest concentrations of $PM_{2.5}$ and WSII components. Totally, concentrations of $PM_{2.5}$ and its components from regional transport during the CLD were much lower than those before (Fig.S7a) and after the CLD (Fig.S7c).

3.4. Formation mechanism of $PM_{2.5}$

As shown in Fig. S8a, NO_3^- was significantly correlated with NH_4^+ (R^2 = 0.85–0.92), suggesting the existential form of NH_4NO_3 (Zhang et al., 2020a, 2020b;). SO_4^{2-} was also correlated with NH_4^+ (R^2 = 0.71–0.80), and the line fit of NH_4^+ and SO_4^{2-} showed a slope of 1.45–2.46 (Fig. S8b), indicating a dominant form of $(NH_4)_2SO_4$ (). In this study, sulfate and nitrate were completely neutralized by ammonium (Fig. S8c). However, there is no significant difference in the existing form of SNA in $PM_{2.5}$ before, during and after the CLD.

Although the CLD reduced the emission of SO_2 and NO_2 to the atmosphere, the changes of SO_4^{2-} and NO_3^- concentrations in $PM_{2.5}$ were obviously different. The variations of SOR and NOR under different periods are shown in Fig. S9. It should be noted that SOR (0.80 ± 0.10) during the CLD was the highest, indicating a high oxidation rate of SO_2. Recent studies found that O_3, H_2O_2, OH, and transition-metal-catalyzed (TMI) O_2 triggered the secondary formation of SO_4^{2-} (Wang et al., 2016; Gen et al., 2019; Li et al., 2020). However, the relative importance of these oxidants enhancing the formation of SO_4^{2-} is still debating. According to RH and T (Table 1), there is no significant difference for meteorological conditions under different pandemic periods. However, O_x was positively correlated with SO_4^{2-} during the CLD (Fig. 5), suggesting the influence of photochemical oxidation. The aqueous phase process of SO_2 oxidation happened much faster, including reactions with O_3, OH, H_2O_2, and organic peroxides (Wang et al., 2016; Gen et al., 2019).

In addition, a good correlation of SO_4^{2-} and Fe and Mn during the CLD was found (Fig. 5). The results showed that the dominance of TMI-catalyzed oxidation for the secondary formation of SO_4^{2-} could be an important pathway under relatively clean conditions. Previous studies had found that SO_2 oxidation catalyzed by transition metals was a dominant in-cloud oxidation pathway (Harris et al., 2013). Li et al. (2020) also reported that TMI played an important role in the rapid formation of sulfate aerosols during haze episodes, contributing to ~50% of total SO_4^{2-} production. Recently, Wang et al. (2021) found that the manganese-catalyzed oxidation of SO_2 during haze events contributed ~70% of the particulate sulfur production, integrating chamber experiments, numerical simulations and in-field observations (Wang et al., 2021). The Mn catalytic reaction rapidly occurred at the aerosol surface layer, and Mn(III) was the intermediate product that could oxidize S(IV) (Wang et al., 2021). Meanwhile, SO_3^- can react with dissolved O_2 to generate SO_5^- radicals, which can oxidize Mn(II) to regenerate Mn(III) (Seinfeld and Pandis, 2016). Therefore, the Mn catalytic redox reaction could continue to produce sulfate while consuming only oxygen and SO_2, meaning that this reaction would occur even in the low concentration of Mn (Wang et al., 2021). Totally, the sulfate production rate was affected by many factors, including the aerosol surface, the aerosol acidity and ionic strength, and environmental conditions (temperature and relative humidity), along with various mixing ratios of SO_2, NO_2 and NH_3 (Hung et al., 2018; Lee et al., 2019; Wang et al., 2021). To evaluate the interaction of sulfate formation and Fe/Mn, we need to calculate the Fe–Mn-catalytic reaction rate under different conditions through chamber experiments. In coastal area, the relative contributions of Fe–Mn-catalytic reaction to secondary formation of SO_4^{2-} should be further studied. In addition, regional transport is also an important factor for enhancing SO_4^{2-}, supported by the PSCF analysis (Fig. 6). As shown in Fig. S7, SO_4^{2-} in the coastal area of southeast China was affected by the long-range sources from urban and industrial areas, including the North China Plain, even during the CLD period.

Figure S10 shows the number size distributions of 7–300 nm particles measured by SMPS during different periods. The average total particle number concentrations of the three-particle modes before the

CLD were 1971 cm^{-3}, 5028 cm^{-3}, and 2372 cm^{-3}, and those during the CLD were 503 cm^{-3}, 1685 cm^{-3}, and 1087 cm^{-3}, respectively. Compared with the pre-epidemic period, the particle number showed a decrease of 74%, 66% and 54%, indicating the influence of anthropogenic emissions. After the CLD, the average total particle number concentrations of the three-particle modes were 1568 cm^{-3}, 2013 cm^{-3}, and 1087 cm^{-3}, respectively. There is evidence for new particle growth before and after the CLD under relatively polluted conditions, yet no continuous and lasting growth from the nucleation-mode particles was observed during the CLD. In addition, the lack of nucleation and particle growth might partly be explained by ambient conditions (e.g., temperature and RH) and concentrations of precursors through local emission and long-range transport.

4. Conclusions

High time resolution characterization and sources apportionment of $PM_{2.5}$ during the COVID-19 pandemic was conducted in a coastal city of southeast China. The average concentrations of various air pollutants, including SO_2, NO_2, $PM_{2.5}$, PM_{10}, OC, EC, and BC, obviously decreased by 27.3%–67.8%, whereas only O_3 increased by 28.1%, reflecting the response of air quality and compositions of $PM_{2.5}$ to the reduction of anthropogenic emissions. Reduced NO_x concentration during the COVID-19 pandemic resulted in O_3 enhancement due to weak titration, further increasing atmospheric oxidation capacity. Under relatively low SO_2 concentrations (1.59 ± 0.97 $\mu g/m^3$), SO_4^{2-} in $PM_{2.5}$ was kept in constant, attributed to the increase of SOR enhanced by transition-metal ion catalyzed and photochemical oxidation. During the city lockdown, the contribution of combustion (33%) and secondary aerosol (31%) to $PM_{2.5}$ increased, while other primary sources including traffic (24%), dust (4.5%), and industry sources (4%) significantly decreased. The results were consistent with the increase of residential activities and fireworks displays and suspending transportations. The levels of regional transported $PM_{2.5}$ and its components during the CLD were relatively low, suggesting the reduction of anthropogenic emissions on a national scale. This study facilitates a better understanding of the effects of emissions control on the formation mechanisms of $PM_{2.5}$ under relatively clean condition.

Declaration of competing interest

The authors declare that they have no known competing financial interests or personal relationships that could have appeared to influence the work reported in this paper.

Acknowledgements

This research was financially supported by the Cultivating Project of Strategic Priority Research Program of Chinese Academy of Sciences (XDPB1903) , the foreign cooperation project of Fujian Province (2020I0038), the Xiamen Youth Innovation Fund Project (3502Z20206094), the FJIRSM&IUE Joint Research Fund (RHZX-2019-006), State Key Laboratory of Environmental Chemistry and Ecotoxicology, Research Center for Eco-Environmental Sciences, CAS (KF2020-06) and center for Excellence in Regional Atmospheric Environment project (E0L1B20201).

Appendix A. Supplementary data

Supplementary data related to this article can be found at https://doi.org/10.1016/j.envpol.2021.117577.

Credit statement

Hong Youwei: Conceptualization, Methodology, Formal analysis, Writing- Original draft preparation, Funding acquisition. Liao Dan, Xu Xinbei: Formal analysis, Writing- Original draft preparation, Data curation. Zheng Ronghua, Ji Xiaoting: Methodology, Resources, Investigation. Xu Lingling, Li Mengren: Software, Validation. Chen Yanting, Wang Hong: Project administration, Visualization. Xiao Hang, Choi Sung-Deuk: Writing- Reviewing and Editing. Chen Jinsheng: Funding acquisition, Writing- Reviewing and Editing.

References

Agrawal, H., Welch, W.A., Miller, J.W., Cocker, D.R., 2008. Emission measurements from a crude oil tanker at sea. Environ. Sci. Technol. 42, 7098–7103.
Bauwens, M., Compernolle, S., Stavrakou, T., Muller, J.F., van Gent, J., Eskes, H., et al., 2020. Impact of coronavirus outbreak on NO(2)Pollution assessed using TROPOMI and OMI observations. Geophys. Res. Lett. 47.
Belis, C.A., Pikridas, M., Lucarelli, F., Petralia, E., Cavalli, F., Calzolai, G., et al., 2019. Source apportionment of fine PM by combining high time resolution organic and inorganic chemical composition datasets. Atmospheric Environment-X 3, 100046-Article No.: 100046.
Chang, Y.H., Huang, R.J., Ge, X.L., Huang, X.P., Hu, J.L., Duan, Y.S., et al., 2020. Puzzling haze events in China during the coronavirus (COVID-19) shutdown. Geophys. Res. Lett. 47.
Chen, L.W.A., Chien, L.-C., Li, Y., Lin, G., 2020. Nonuniform impacts of COVID-19 lockdown on air quality over the United States. Sci. Total Environ. 745, 141105-141105.
Collivignarelli, M.C., Abba, A., Bertanza, G., Pedrazzani, R., Ricciardi, P., Miino, M.C., 2020. Lockdown for CoViD-2019 in Milan: what are the effects on air quality? Sci. Total Environ. 732.
Ding, A., Huang, X., Nie, W., Chi, X., Xu, Z., Zheng, L., et al., 2019. Significant reduction of $PM_{2.5}$ in eastern China due to regional-scale emission control: evidence from SORPES in 2011-2018. Atmos. Chem. Phys. 19, 11791–11801.
Gen, M., Zhang, R., Huang, D.D., Li, Y., Chan, C.K., 2019. Heterogeneous SO_2 oxidation in sulfate formation by photolysis of particulate nitrate. Environ. Sci. Technol. Lett. 6, 86–91.
Han, L.H., Zhuang, G.S., Cheng, S.Y., Wang, Y., Li, J., 2007. Characteristics of re-suspended road dust and its impact on the atmospheric environment in Beijing. Atmos. Environ. 41, 7485–7499.
Harris, E., Sinha, B., van Pinxteren, D., Tilgner, A., Fomba, K.W., Schneider, J., et al., 2013. Enhanced role of transition metal ion catalysis during in-cloud oxidation of SO_2. Science 340, 727–730.
He, G.J., Pan, Y.H., Tanaka, T., 2020. The short-term impacts of COVID-19 lockdown on urban air pollution in China. Nature Sustainability 3, 1005–1011.
Hopke, P.K., Barrie, L.A., Li, S.M., Cheng, M.D., Li, C., Xie, Y., 1995. Possible sources and preferred pathways for biogenic and non-sea-salt sulfur for the high arctic. Journal of Geophysical Research-Atmospheres 100, 16595–16603.
Hu, B., Liu, T., Hong, Y., Xu, L., Li, M., Wu, X., et al., 2020. Characteristics of peroxyacetyl nitrate (PAN) in a coastal city of southeastern China: photochemical mechanism and pollution process. Sci. Total Environ. 719.
Huang, X., Ding, A., Gao, J., Zheng, B., Zhou, D., Qi, X., et al., 2020a. Enhanced secondary pollution offset reduction of primary emissions during COVID-19 lockdown in China. National Science Review.
Huang, X., Ding, A.J., Wang, Z.L., Ding, K., Gao, J., Chai, F.H., et al., 2020b. Amplified transboundary transport of haze by aerosol-boundary layer interaction in China. Nat. Geosci. 8 (2), 137–145.
Hung, H.M., Hsu, M.N., Hoffmann, M.R., 2018. Quantification of SO_2 oxidation on interfacial surfaces of acidic micro-droplets: implication for ambient sulfate formation. Environ. Sci. Technol. 52, 9079–9086.
Jia, H., Huo, J., Fu, Q., Duan, Y., Lin, Y., Jin, X., et al., 2020. Insights into chemical composition, abatement mechanisms and regional transport of atmospheric pollutants in the Yangtze River Delta region, China during the COVID-19 outbreak control period. Environ. Pollut. 267.
Kong, S.F., Li, L., Li, X.X., Yin, Y., Chen, K., Liu, D.T., et al., 2015. The impacts of firework burning at the Chinese Spring Festival on air quality: insights of tracers, source evolution and aging processes. Atmos. Chem. Phys. 15, 2167–2184.
Kraemer, M.U.G., Yang, C.H., Gutierrez, B., Wu, C.H., Klein, B., Pigott, D.M., et al., 2020. The effect of human mobility and control measures on the COVID-19 epidemic in China. Science 368, 493-+.
Le, T., Wang, Y., Liu, L., Yang, J., Yung, Y.L., Li, G., et al., 2020. Unexpected air pollution with marked emission reductions during the COVID-19 outbreak in China. Science 369, 702–706.
Lee, J.K., et al., 2019. Spontaneous generation of hydrogen peroxide from aqueous microdroplets. Proc. Natl. Acad. Sci. U.S.A. 116, 19294–19298.
Li, J.H.Y., Zhang, Y.L., Cao, F., Zhang, W.Q., Fan, M.Y., Lee, X.H., et al., 2020. Stable sulfur isotopes revealed a major role of transition-metal ion-catalyzed SO_2 oxidation in haze episodes. Environ. Sci. Technol. 54, 2626–2634.
Liu, F., Page, A., Strode, S.A., Yoshida, Y., Choi, S., Zheng, B., et al., 2020a. Abrupt decline in tropospheric nitrogen dioxide over China after the outbreak of COVID-19. Science Advances 6.
Liu, S., Xing, J., Zhao, B., Wang, J., Wang, S., Zhang, X., et al., 2019a. Understanding of aerosol-climate interactions in China: aerosol impacts on solar radiation, temperature, cloud, and precipitation and its changes under future climate and emission scenarios. Current Pollution Reports 5, 36–51.

Liu, T., Hu, B., Yang, Y., Li, M., Hong, Y., Xu, X., et al., 2020b. Characteristics and source apportionment of $PM_{2.5}$ on an island in Southeast China: impact of sea-salt and monsoon. Atmos. Res. 235.
Miyazaki, K., Bowman, K., Sekiya, T., Jiang, Z., Chen, X., Eskes, H., et al., 2020. Air quality response in China linked to the 2019 novel coronavirus (COVID-19) lockdown. Geophys. Res. Lett. 47.
Pei, Z., Han, G., Ma, X., Su, H., Gong, W., 2020. Response of major air pollutants to COVID-19 lockdowns in China. Sci. Total Environ. 743.
Polissar, A.V., Hopke, P.K., Paatero, P., Kaufmann, Y.J., Hall, D.K., Bodhaine, B.A., et al., 1999. The aerosol at Barrow, Alaska: long-term trends and source locations. Atmos. Environ. 33, 2441–2458.
Polissar, A.V., Hopke, P.K., Paatero, P., 1998. Atmospheric aerosol over Alaska - 2. Elemental composition and sources. Journal of Geophysical Research-Atmospheres 103, 19045–19057.
Rodriguez-Urrego, D., Rodriguez-Urrego, L., 2020. Air quality during the COVID-19: $PM_{2.5}$ analysis in the 50 most polluted capital cities in the world. Environ. Pollut. 266.
Saraswat, R., Saraswat, D.A., 2020. Research opportunities in pandemic lockdown. Science 368, 594–595.
Seinfeld, J.H., Pandis, S.N., 2016. Atmospheric Chemistry and Physics: from Air Pollution to Climate Change. John Wiley & Sons.
Sharma, S., Zhang, M.Y., Anshika, Gao, J.S., Zhang, H.L., Kota, S.H., 2020. Effect of restricted emissions during COVID-19 on air quality in India. Sci. Total Environ. 728.
Singh, V., Singh, S., Biswal, A., Kesarkar, A.P., Mor, S., Ravindra, K., 2020. Diurnal and temporal changes in air pollution during COVID-19 strict lockdown over different regions of India. Environ. Pollut. 266.
Stratoulias, D., Nuthammachot, N., 2020. Air quality development during the COVID-19 pandemic over a medium-sized urban area in Thailand. Sci. Total Environ. 746, 141320-141320.
Su, H., Cheng, Y., Poschl, U., 2020. New multiphase chemical processes influencing atmospheric aerosols, air quality, and climate in the anthropocene. Accounts Chem. Res. 53 (10), 2034–2043.
Sun, Y., Lei, L., Zhou, W., Chen, C., He, Y., Sun, J., et al., 2020. A chemical cocktail during the COVID-19 outbreak in Beijing, China: insights from six-year aerosol particle composition measurements during the Chinese New Year holiday. Sci. Total Environ. 742, 140739-140739.
Tao, J., Zhang, L.M., Cao, J.J., Zhong, L.J., Chen, D.S., Yang, Y.H., et al., 2017. Source apportionment of $PM_{2.5}$ at urban and suburban areas of the Pearl River Delta region, south China - with emphasis on ship emissions. Sci. Total Environ. 574, 1559–1570.
Tian, H.Y., Liu, Y.H., Li, Y.D., Wu, C.H., Chen, B., Kraemer, M.U.G., et al., 2020. An investigation of transmission control measures during the first 50 days of the COVID-19 epidemic in China. Science 368, 638.
Wang, G.H., Zhang, R.Y., Gomez, M.E., Yang, L.X., Zamora, M.L., Hu, M., et al., 2016. Persistent sulfate formation from London Fog to Chinese haze. Proc. Natl. Acad. Sci. U.S.A. 113, 13630–13635.
Wang, J., Li, J., Ye, J., Zhao, J., Wu, Y., Hu, J., et al., 2020a. Fast sulfate formation from oxidation of SO_2 by NO_2 and HONO observed in Beijing haze. Nat. Commun. 11.
Wang, J., Wang, S., Jiang, J., Ding, A., Zheng, M., Zhao, B., et al., 2014. Impact of aerosol-meteorology interactions on fine particle pollution during China's severe haze episode in January 2013. Environ. Res. Lett. 9.
Wang, Y., Yuan, Y., Wang, Q., Liu, C., Zhi, Q., Cao, J., 2020b. Changes in air quality related to the control of coronavirus in China: implications for traffic and industrial emissions. Sci. Total Environ. 731.
Wang, W., Liu, M., Wang, T., et al., 2021. Sulfate formation is dominated by manganese-catalyzed oxidation of SO_2 on aerosol surfaces during haze events. Nat. Commun. 12, 1993. https://doi.org/10.1038/s41467-021-22091-6.
Watson, J.G., Chow, J.C., Houck, J.E., 2001. $PM_{2.5}$ chemical source profiles for vehicle exhaust, vegetative burning, geological material, and coal burning in Northwestern Colorado during 1995. Chemosphere 43, 1141–1151.
Wu, X., Li, M., Chen, J., Wang, H., Xu, L., Hong, Y., et al., 2020. The characteristics of air pollution induced by the quasi-stationary front: formation processes and influencing factors. Sci. Total Environ. 707.
Wu, X., Xu, L.L., Hong, Y.W., Chen, J.F., Qiu, Y.Q., Hu, B.Y., et al., 2019. The air pollution governed by subtropical high in a coastal city in Southeast China: formation processes and influencing mechanisms. Sci. Total Environ. 692, 1135–1145.
Xu, L., Jiao, L., Hong, Z., Zhang, Y., Du, W., Wu, X., et al., 2018. Source identification of PM2.5 at a port and an adjacent urban site in a coastal city of China: impact of ship emissions and port activities. Sci. Total Environ. 634, 1205–1213.
Yu, Y., He, S., Wu, X., Zhang, C., Yao, Y., Liao, H., et al., 2019. $PM_{2.5}$ elements at an urban site in Yangtze River Delta, China: high time-resolved measurement and the application in source apportionment. Environ. Pollut. 253, 1089–1099.
Zangari, S., Hill, D.T., Charette, A.T., Mirowsky, J.E., 2020. Air quality changes in New York City during the COVID-19 pandemic. Sci. Total Environ. 742.
Zhang, Q., Zheng, Y., Tong, D., Shao, M., Wang, S., Zhang, Y., et al., 2019. Drivers of improved $PM_{2.5}$ air quality in China from 2013 to 2017. Proc. Natl. Acad. Sci. U.S.A. 116, 24463–24469.
Zhang, Y., Hong, Z., Chen, J., Xu, L., Hong, Y., Li, M., et al., 2020a. Impact of Control Measures and Typhoon Weather on Characteristics and Formation of $PM_{2.5}$ during the 2016 G20 Summit in China. Atmospheric Environment, p. 224.
Zhang, Y., Xu, L., Zhuang, M., Zhao, G., Chen, Y., Tong, L., et al., 2020b. Chemical composition and sources of submicron aerosol in a coastal city of China: results from the 2017 BRICS summit study. Sci. Total Environ. 741, 140470-140470.
Zhang, Y., Zhang, H., Deng, J., Du, W., Hong, Y., Xu, L., et al., 2017b. Source regions and transport pathways of $PM_{2.5}$ at a regional background site in East China. Atmos. Environ. 167, 202–211.
Zheng, G., Su, H., Wang, S., Andreae, M.O., Poschl, U., Cheng, Y., 2020a. Multiphase buffer theory explains contrasts in atmospheric aerosol acidity. Science (New York, N.Y.) 369, 1374–1377.
Zhao, N., Wang, G., Li, G., Lang, J., Zhang, H., 2020. Air pollution episodes during the COVID-19 outbreak in the Beijing-Tianjin-Hebei region of China: an insight into the transport pathways and source distribution. Environ. Pollut. 267.
Zheng, H., Kong, S., Chen, N., Yan, Y., Liu, D., Zhu, B., et al., 2020b. Significant changes in the chemical compositions and sources of $PM_{2.5}$ in Wuhan since the city lockdown as COVID-19. Sci. Total Environ. 739, 140000-140000.
Zheng, M., Yan, C., Zhu, T., 2020c. Understanding sources of fine particulate matter in China. Phil. Trans. Math. Phys. Eng. Sci. 378.